Journal of Materials Chemistry C

RSC Publishing

PAPER

View Article Online
View Journal | View Issue



Cite this: J. Mater. Chem. C, 2013, 1, 3825

# A UV-ozone treated amorphous barium–strontium titanate dielectric thin film for low driving voltage flexible organic transistors

Zongrong Wang,[a] Xiaochen Ren,[b] Chi Wah Leung,[c] Sanqiang Shi[a] and Paddy Kwok Leung Chan*[b]

Received 22nd February 2013
Accepted 15th April 2013

DOI: 10.1039/c3tc30345d

www.rsc.org/MaterialsC

Reducing the operating power and making them suitable for portable and wearable electronic applications are critical steps for the further development of organic field effect transistors (OFETs). One of the possible approaches to achieve this is by using a high dielectric constant (high-*k*) dielectric layer. Here, we propose a new kind of high-*k* amorphous $Ba_{0.7}Sr_{0.3}TiO_3$ (BST) material derived by a layer-by-layer sol–gel method and solidified by UV-ozone treatments under atmospheric air and pressure. The dielectric constant of the amorphous BST thin film is around 11. Without employing the self-assembled monolayers (SAMs), the pentacene OFET on a polyethylene naphthalate (PEN) substrate shows saturation under −2.5 V, the saturation mobility of 0.252 $cm^2\ V^{-1}\ s^{-1}$ with negligible hysteresis effects. The chemical composition of the dielectric film and the morphology structure are studied by X-ray photoelectron spectroscopy (XPS) and atomic force microscopy (AFM) respectively. We also performed compressive and tensile bending tests on the OFETs and the dielectric layer. Due to the amorphous nature of the BST thin film, it shows a constant *C–f* relationship in both compressive and tensile bending up to a bending radius of 3.3 mm. It demonstrates high application potential of the current BST thin film in flexible electronics and circuits. To confirm the application potentials, we develop an organic inverter based on the transistor and a resistor, and a gain as high as 20 can be achieved.

## Introduction

Organic field effect transistors (OFETs) play an important role in many new generations of organic electronic devices, such as memories, bio-sensors, displays, drivers and radio frequency identification (RFID).[1–5] One of the major challenges in producing these devices is to reduce the operating power for the portable or wearable electronic applications and make them compatible with dry cell powering. In the applications of OFETs, low operating power means sufficient charges can accumulate at the semiconductor–dielectric interface to generate a conductive channel under a small voltage bias at the gate. The density of the induced charges $\Delta n$ is proportional to the areal capacitance of the dielectric insulator ($C'$) and is given by:

$$\Delta n = (V_G - V_{th})C'/q \quad (1)$$

where $V_G$, $V_{th}$ and $q$ are the gate bias, threshold voltage and the electronic charge, respectively. To maintain $\Delta n$ at sufficiently large value while $V_G - V_{th}$ is small for low power operating, the areal capacitances of the dielectric thin films have to be large. Depending on the charge mobility of the organic semiconductors and other geometry parameters of the OFET, the dielectric film usually requires large areal capacitance such that the operating voltage can be less than 5 V. One of the possible methods to increase $C'$ is by reducing the thickness of the dielectric layer, such as the ultrathin 3 nm thick hafnium oxide ($HfO_x$) layer reported by Jen *et al.*[6] A common drawback of ultrathin dielectrics is a high leakage current through the gate which deteriorates the device performance. To alleviate the defects, SAMs are usually employed.[6–11] However, the functional head groups of SAMs are usually surface specific which limits their applications on arbitrary dielectrics or gate electrodes. For example on $SiO_2$, strong Si–O–Si bonds connect the precursor silane to the surface silanol (–Si–OH) groups.[9] On the other hand, noble metals require SAMs with alkanethiol head groups to form monolayers on the surface directly.[10] Alternatively, the operating power of OFETs can be reduced by using high-*k* dielectric materials. The deposition of high-*k* materials can be achieved by various methods as summarized in Table 1. They can be divided into physical methods (such as atomic layer

[a]Department of Mechanical Engineering, The Hong Kong Polytechnic University, Kowloon, Hong Kong. E-mail: mmsqshi@polyu.edu.hk

[b]Department of Mechanical Engineering, The University of Hong Kong, Pokfulam, Hong Kong. E-mail: pklc@hku.hk

[c]Department of Applied Physics, The Hong Kong Polytechnic University, Kowloon, Hong Kong. E-mail: apleung@polyu.edu.hk

**Table 1** Summary of various methods for fabricating low voltage OFETs

| Method | | Material | Environment | Temperature (°C) | Substrate |
|---|---|---|---|---|---|
| Physical methods | Atomic layer deposition | $Al_2O_3$ (ref. 12) | $N_2$ or Ar | 100 | ITO glass |
| | | $HfO_2$ (ref. 13) | $H_2O$ vapor | 200 | n+ silicon |
| | | $HfO_2$ + BCB (ref. 14) | Vapor for $HfO_2$<br>$N_2$ for BCB | 200 for $HfO_2$<br>250 for BCB | n+ silicon |
| | Pulsed laser deposition | BST (ref. 15) | Vacuum | 110 | PEN |
| | Oxygen plasma + SAM | $AlO_x$ (ref. 3) | Air | RT | PEN |
| | RF magnetron sputtering | BZT (ref. 16) | $Ar/O_2$ | RT | PC |
| Solution methods | Sol–gel + heat treatment | $HfO_x$ (ref. 6) | NA | 600 | n+ silicon |
| | | BTO (ref. 17) | Air | 180 | Glass |
| | Chemical solution | BST (ref. 18) | $O_2$ | 400 | $Pt/Ti/SiO_2/Si$ |
| | Sol–gel + UV-ozone | $ZrO_x$ (ref. 11) | Air | RT | n+ silicon |
| | Spin-coating | P(VDF-TrFE-CFE) (ref. 19) | $N_2$ | 60 | PET |
| | Spin-coating | P(VDF-TrFE) + PVP (ref. 20) | Air for P(VDF-TrFE)<br>Vacuum for PVP | RT for P(VDF-TrFE)<br>175 for PVP | PES |

deposition (ALD), pulsed laser deposition (PLD), sputtering or oxygen plasma) and solution methods (such as sol–gel processing and direct spin coating). Although vacuum environment or expensive deposition equipment may not be required for solution methods, inert environment (for high-*k* polymer dielectric) or high temperature annealing (annealing temperature of the traditional high-*k* dielectric formed by a sol–gel method ranges from 180 °C (ref. 17) to as high as 600 °C (ref. 6)) may still be necessary, and thus they are not compatible with ambient air and low temperature deposition. Recently, a new UV-ozone dielectric treatment method has been proposed for high quality sol–gel thin film fabrication. Jen and coauthors have fabricated an ultrathin $HfO_x$ film of 5 nm on both silicon and Kapton substrate for OFET applications. However, the processing temperature is still relatively high at 200 °C, which is higher than the glass transition temperature of various polymer flexible substrates.[21] Besides, Salleo *et al.* have also reported ultrathin $ZrO_x$ of 6–7 nm on silicon by using a wide range of UV light, including UVA, UVB and UVV, and ozone is proposed to oxidize the thin film at room temperature. The OFET shows high performance with an operating voltage of less than 3 V.[11] Since the thicknesses of both $HfO_x$ and $ZrO_x$ are less 10 nm, the device would be sensitive to the surface roughness of the substrate. As a result, SAMs were deposited onto these ultrathin dielectric films to suppress the leakage current in the OFET applications.

Here we propose a new kind of high-*k* amorphous barium–strontium titanate (BST) material derived by a layer-by-layer sol–gel method and solidified by UV-ozone treatments under ambient air. We separated the thermal annealing effect in the UV-ozone treatment by performing pure thermal annealing on the samples under ambient air without UV-ozone. The dielectric constant of the amorphous BST thin film is around 11 (after considering the contribution from the $AlO_x$ on the Al gate electrode). Without the self-assembled monolayer, the pentacene OFET on a PEN substrate shows saturation under −2.5 V, the saturation mobility of 0.252 $cm^2\ V^{-1}\ s^{-1}$ and negligible hysteresis effects. The chemical composition of the dielectric thin film is identified by comparing the individual peaks in the X-ray photoelectron spectroscopy (XPS) measurements. The dielectric properties of the device as well as the performance of the OFET on PEN substrates at different bending radii were also investigated. The capacitance–frequency measurements of the dielectric film show no observable change under both conditions of compressive and tensile strain even at a bending radius of 3.3 mm, suggesting that the amorphous BST on Al is an excellent candidate for the dielectric insulator in ultra-flexile electronics. Furthermore, similar OFET performances on both silicon and PEN substrates represent the current low temperature and UV-ozone treated amorphous BST films can be used as high-*k* dielectric materials without using SAMs.

## Experimental section

To prepare the sol precursor for the BST thin films, $Ba(CH_3COO)_2\cdot 2H_2O$, $Sr(NO_3)_2$, and $Ti(C_4H_9O)_4$ were used as raw materials. Acetylacetone (AcAc) was used as a complexing agent and ethylene glycol monomethyl ether along with ethylene glycol as solvents. The Ba/Sr ratio of the BST thin film was set as 0.7/0.3 by controlling the raw materials. Firstly, $Ba(CH_3COO)_2\cdot 2H_2O$ and $Sr(NO_3)_2$ with a molar ratio of 0.7 : 0.3 were dissolved in mixed solvents of ethylene glycol and ethylene glycol monomethyl ether and heated to 110 °C to obtain a Ba–Sr solution. $Ti(C_4H_9O)_4$ was diluted in the mixture of solvents of ethylene glycol monomethyl ether and ethylene glycol with complexing agent AcAc to prepare Ti solution at room temperature. Nitric acid was introduced to prevent the hydrolyzation of Ti. Finally, the cooled down Ba–Sr solution was added to the obtained Ti sol mixture to prepare the final (Ba–Sr)–Ti sol precursors. The concentration was controlled to be about 0.1 mol $L^{-1}$ in molarity of BST.

The BST sol precursors were deposited on both n++ silicon (University wafer) and PEN substrates (Goodfellow, 125 μm) with 60 nm evaporated Al electrode by a spin coating method. The silicon substrate was etched in HF and cleaned in deionized water, acetone and isopropanol, by ultrasonication, respectively. The PEN substrates were also cleaned by the organic solvents. Before the PEN substrate was put into chamber for the bottom Al electrode evaporation, the PEN was put into the UV-ozone chamber (Jelight Model 42-220 and the power is

 

28–32 mW $cm^{-2}$) for 5 minutes for surface cleaning. The rotation speed was 4000 rpm for two solution drops for each layer. The rotation time for the first drop was 10 seconds and 30 seconds for the second drop. After the spin coating, the wet films were treated in an air atmosphere by UV-ozone. Totally three layers of BST were deposited and the UV-ozone treatment time was 30 minutes for the first layer and 10 minutes for the following two layers.

The pentacene OFET devices were fabricated by 40 nm pentacene thermally evaporated on top of the BST thin film directly after the UV-ozone treatment. The top source and drain electrodes were thermally evaporated through mechanical shadow masks. The capacitor devices were structured with the BST thin film sandwiched between the bottom Al electrode and top Ag electrode. All electrodes were deposited by thermal evaporation.

## Results and discussion

Fig. 1(a) shows a picture of the OFET and the schematic structure of the device on a flexible PEN substrate. A transmission electron microscope (TEM, Philips Tecnai G220 S-TWIN) was used to characterize the crystallization behavior and the actual thickness of the BST thin film on the n++ silicon electrode. Fig. 1(b) shows the cross-sectional images of the dielectric stack in different regions of the Al gate electrode (60 nm) and silicon substrate. It can be noticed from the enlarged TEM image that there are thin layers of $AlO_x$ and $SiO_2$ on the Al gate electrode and silicon substrate, respectively. The oxide layers are believed to be formed during the UV-ozone treatment of the BST layer, similar to the observations reported in ref. 21 and 22. The effective capacitance of the dielectric can be considered as two capacitors: BST and $AlO_x$ are connected in series. By knowing the equivalent areal capacitance (300 nF $cm^{-2}$), the thicknesses of BST (28 nm) and $AlO_x$ (4 nm), and the dielectric constant of the reported ultrathin $AlO_x$ ($\varepsilon = 7.8\varepsilon_0$),[23] the dielectric constant of the BST is evaluated to be around 11. It is important to point out that the current UV-ozone treatment method would unavoidably form a thin oxide layer on the gate electrode. This thin layer of oxide would reduce the leakage current of the device. Electrodes, which can form a stable oxide thin film such as Al and Ni, would be applicable.

To eliminate the thermal effects during the UV-ozone treatment, we measured the temperature of the samples under UV-ozone treatment by thermocouples and the maximum temperature that can be achieved in the whole process is 85 °C. We then fabricate transistors with the BST solution spin-coated on an Al bottom electrode and annealed on a hot plate under air with the same temperature profile for the same period of time (50 min) without UV-ozone. The devices do not work as normal transistors but show large leakage current which confirms the UV-ozone treatment is dominating over the thermal annealing effect in our current devices. Different from the high temperature annealed BST thin film, it is important to point out that the current UV-ozone treated BST layer shows no diffraction lattice structure which shows the amorphous nature of the film, which will result in a lower dielectric constant.

The as prepared BST thin film was studied by XPS (Physical Electrics 5600 multi-technique system, Versa Probe II Scanning XPS) to verify the chemical states of different elements in the

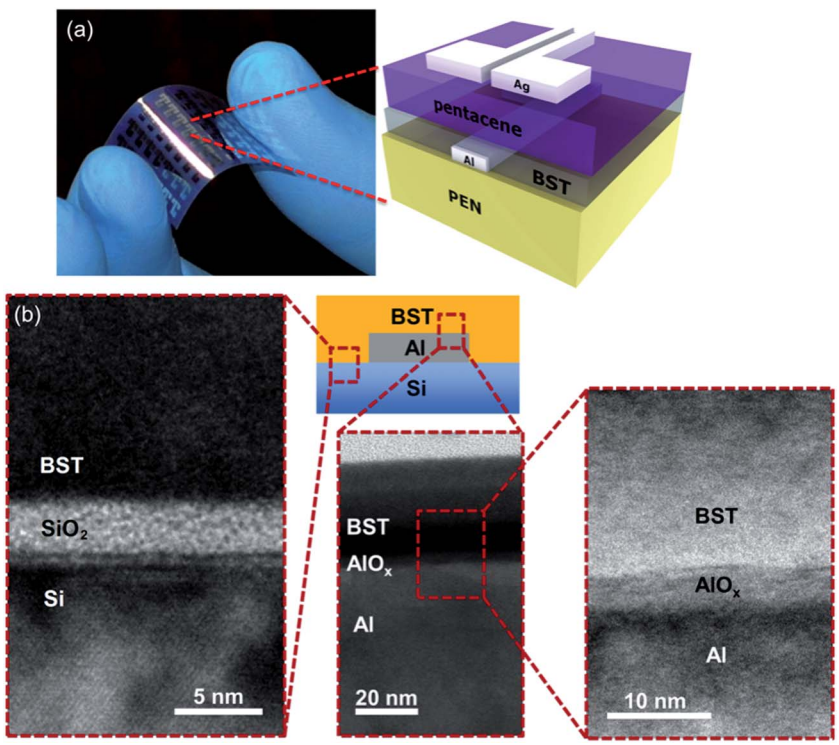


**Fig. 1** (a) Schematic structure of the OFET device on a PEN substrate. (b) Cross-sectional TEM of the BST thin film on the silicon substrate and Al bottom electrode.

thin film. Fig. 2 shows the survey scan of the BST thin film. The black, red and blue curves represent the as prepared BST thin film, and the BST thin film after the first and second argon ion etching processes, respectively. The binding energy peaks of the three curves almost coincide. The identical peaks in two curves after the first and the second ion milling suggest that the composition of the film is uniform. The four elements (Sr, Ti, O and Ba) were investigated separately, from low to high binding energy in the survey scan curves as shown in Fig. 2(b)–(e). By using the individual peak areas and sensitivity factors from XPS quantitative analysis data, the molar proportion of this BST thin film could be evaluated as $Ba_{0.62}Sr_{0.28}TiO_{3.03}$, which is quite close to the raw material ratio as discussed in the Experimental section. The peaks at around 134.3 eV and 136.1 eV are attributed to Sr 3d, as shown in Fig. 2(b). The binding energies of these two peaks are slightly larger than the Sr 3d peak value (133 eV) in ref. 24 in which the $SrTiO_3$ is hydrothermally treated at 245 °C. The higher binding energy is believed to be due to the ozone effect, which converts the elements to the oxidized state, resulting in fewer electrons in the outer orbitals and thus higher binding energy. The binding energy values of the peaks for titanium, oxygen and barium in Fig. 2(c)–(e) are comparable with the experimental findings in ref. 25, 26 and 17, respectively. Different from the high temperature annealing process which requires purging of high purity oxygen during the annealing, the current UV-ozone treated BST thin film shows

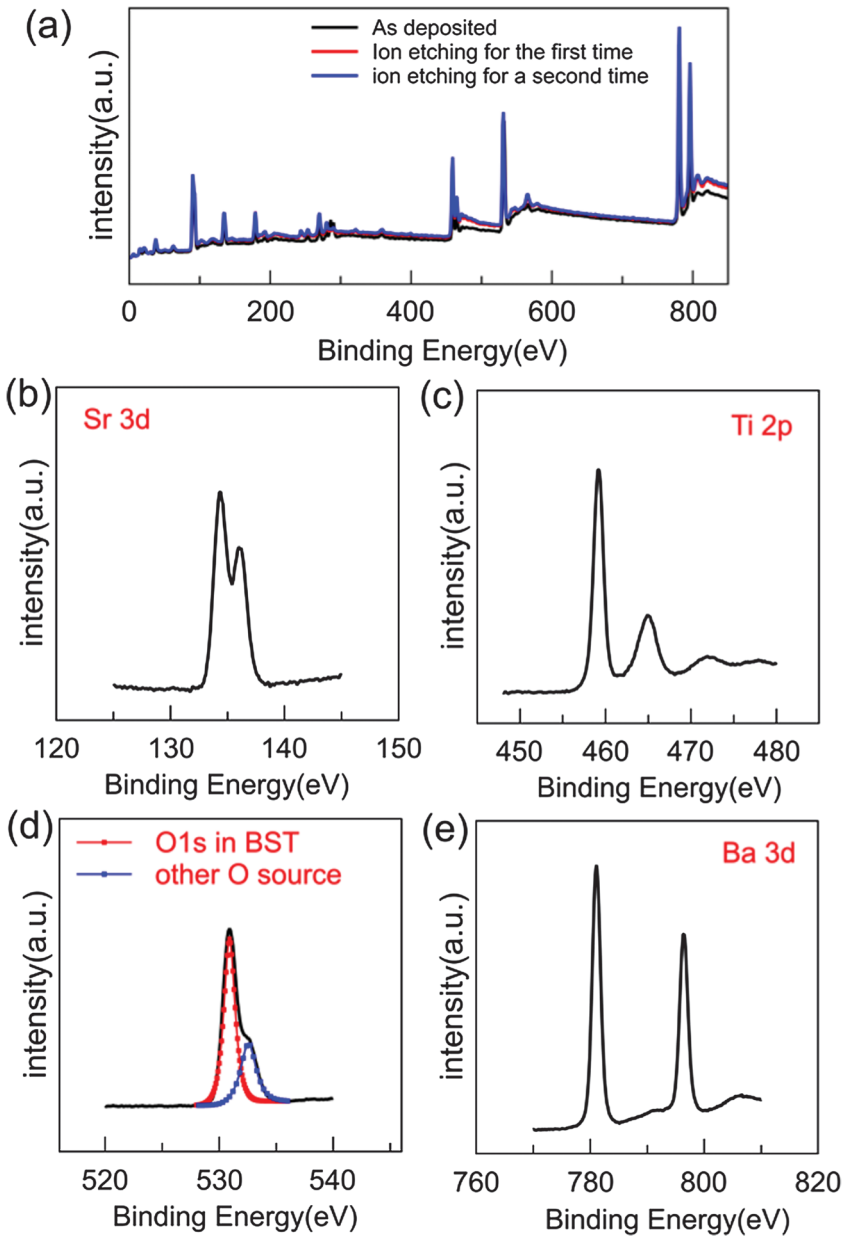


**Fig. 2** (a) X-ray photoelectron spectroscopy (XPS) survey scan of the BST thin film derived by a sol–gel method and UV-ozone treatment. (b) XPS core level spectra of Sr 3d. (c) XPS core level spectra of Ti 2p. (d) XPS core level spectra of O 1s. (e) XPS core level spectra of Ba 3d.

 

similar XPS peak values, which suggests that UV-ozone treatment on the sol–gel film is an alternative method to form high quality dielectrics as it can fill up the oxygen vacancies within the film.[21] As the UV-ozone machine emits 184.9 nm and 253.7 nm under ambient air conditions, it will convert oxygen into reactive O species ($O(^1D)$). The reactive oxygen atom will then diffuse into the amorphous BST thin film and react with the oxygen vacancies in the film ($V^{2-}$) to form lattice oxygen:[21,27]

$$O(^1D) + V^{2-} \rightarrow O^{2-} \quad (2)$$

Other than filling up the oxygen vacancy defects in the BST thin film, the reactive oxygen would also remove the organic impurities in the film, which results in a high quality amorphous BST thin film with better stoichiometry.[21]

To verify whether the thin film can be exploited to OFET devices, we examine the surface morphology of the Al bottom electrode, BST thin film on Al and the pentacene on top of the BST thin film by atomic force microscopy (AFM) as shown in Fig. 3. The root mean square (RMS) roughness of the Al electrode and of the BST thin film on top of Al are 5.9 nm and 3.3 nm, respectively. The thermally evaporated pentacene thin film (40 nm) on top of the BST thin film shows grain size larger than 1 μm, and layer-by-layer structure (Fig. 3(d)). This corresponds to the Stranski–Krastanov (S–K) growth mode and it is expected to provide higher carrier mobility in the channel region of the OFETs.

In the fabrication of the transistor, after the deposition of the pentacene layer on the amorphous BST dielectric, source and drain electrodes are grown through mechanical shadow masks and the channel width and length are 2000 μm and 100 μm, respectively. Detailed fabrication steps are discussed in the Experimental section. The device performance on both silicon and PEN is shown in Fig. 4. On the silicon substrate, the transistor device shows a mobility, threshold voltage ($V_{th}$) and sub-threshold swing (SS) of 0.289 $cm^2 V^{-1} s^{-1}$, −1.18 V and 140 mV $dec^{-1}$, respectively. For the PEN device, the saturation field effect mobility is 0.252 $cm^2 V^{-1} s^{-1}$, the $V_{th}$ equals −1.16 V and SS equals 150 mV $dec^{-1}$. In Fig. 5, we compared the thin film pentacene carrier mobility of flexible OFETs with various dielectric materials (only consider (i) pentacene, (ii) flexible substrate, and (iii) single layer of dielectric without SAM or other further treatment). The pentacene mobility obtained in the current work is comparable with the commonly solution-processed polymer dielectric (including both high-*k* and low-*k*) such as benzocyclobutene (BCB),[28] polyimide (PI),[29] poly(methyl methacrylate) (PMMA),[30] polyvinyl-phenol (PVP),[31] CPVP-$C_6$,[32] and P(VDF-TrFE-CFE).[19] Although the dielectric constant of the current amorphous BST thin film is lower than the chemically processed (anodization) $Ta_2O_5$, the pentacene carrier mobility can be maintained at a similar level.[33] In Fig. 5, we also compare other non-polymer high-*k* dielectrics developed by the physical methods such as $TiSiO_2$ derived by RF sputtering,[34] or BST[15] and BZN derived by PLD.[35] In this work, different from typical physical methods which require valuable equipment, we demonstrated that the metal oxide high-*k* dielectric material

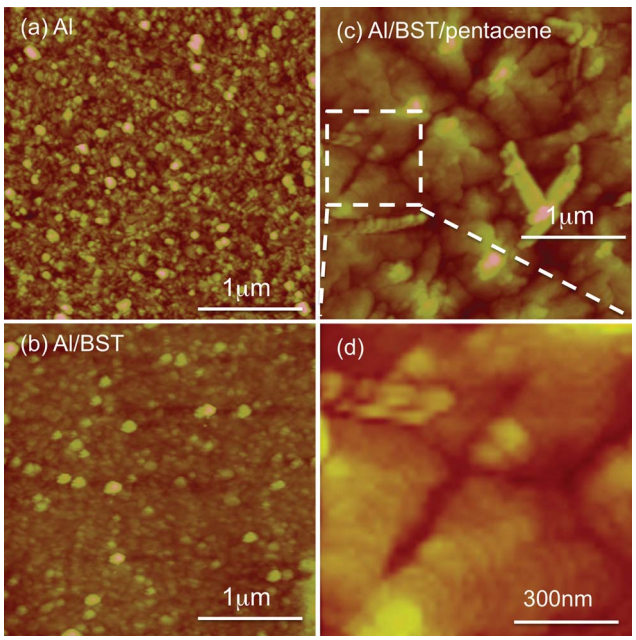


**Fig. 3** (a) AFM image of Al bottom gate electrode on PEN substrate. (b) BST on top of Al electrode. (c) Pentacene thermally evaporated on top of BST. (d) The magnified AFM image of the pentacene crystal highlighted in (c).

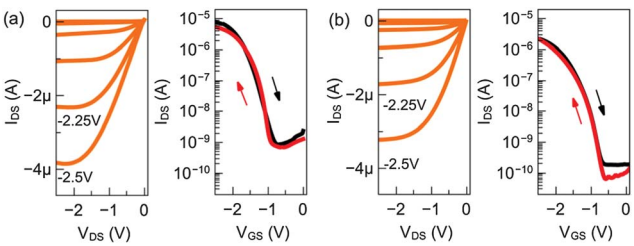


**Fig. 4** (a) The output (with $V_{GS}$ ranging from 0 to −2.5 V with a step of 0.25 V) and transfer curves ($V_{DS}$ = −2.5 V) for OFETs on a Si substrate. The mobility, $V_{th}$, and sub-threshold swing are 0.289 $cm^2 V^{-1} s^{-1}$, −1.18 V and 140 mV $dec^{-1}$, respectively. (b) The output and transfer curves of OFETs on PEN. The mobility, $V_{th}$ and sub-threshold swing are 0.252 $cm^2 V^{-1} s^{-1}$, −1.16 V and 150 mV $dec^{-1}$, respectively. The higher off current in the Si substrate device is attributed to the unpatterned gate electrode.

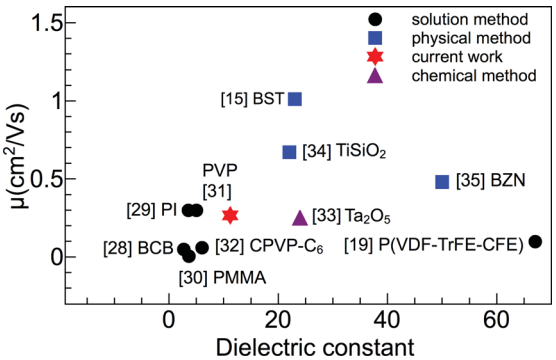


**Fig. 5** The comparison between the mobility of different flexible pentacene OFETs and the current work.

can be applied directly under ambient air conditions by solution processing without vacuum requirement, SAM deposition, and post-annealing treatment. It is important to mention that although the carrier mobility of the solution processed dielectric device is not among the highest when compared with other methods like physical deposition or chemical deposition, it is still higher than the benchmark mobility of 0.1 $cm^2 V^{-1} s^{-1}$ and sufficient for commercial exploitation[36] especially in large area deposition where the solution processing technique has significant advantages.

In the practical application of the BST dielectric in flexible electronics, it is important to study the performance of the OFETs under bending. We investigated the performance of the OFETs by concave (downward) and convex (upward) bending at different radii. The downward and upward bending introduce compressive and tensile strain to the device, respectively. The centralized line of the strain will be in the PEN substrate as its thickness is three orders of magnitude larger than the active layers. Fig. 6(a) and (b) show the variation of the normalized saturation mobility and the threshold voltage of the device at different bending radii in downward bending and upward bending, respectively. The results are obtained on a fresh device which has not been used for any bending test before. The filled circles indicate the values without bending and the testing setup is shown in Fig. 6(c). It can be noticed that the variation of $V_{th}$ and mobility are not significant in the convex bending test. However, in concave bending (compressive strain), the mobility of the device shows a more obvious increase then decrease trend while the threshold voltage is relatively stable. Two factors may have caused the increase in mobility under compressive strain: it can be due to shorter distance between the pentacene molecules, which thus favors the hopping mechanism of the holes in the channel, or it can be due to the change of charge density in the channel resulting from the variation of the areal capacitance.[37] To further investigate the mechanism causing the mobility variation under strain, we independently examined the dielectric properties of the BST layer under both compressive and tensile strains without the pentacene layer. Similar to the OFET device, the capacitance of the gate dielectric layer of BST was investigated at different bending radii. The amorphous BST thin film was sandwiched between the bottom Al electrode and the top Ag electrode for the capacitance measurement. Fig. 7(a) and (b) show the results of the *C–f* measurements for downward and upward bending, respectively. From these two figures, it can be clearly observed that the capacitance–frequency of the BST layer at different bending radii is almost constant in the whole measurement frequency range. This observation is different from the polymer dielectric, in which Bao *et al.* have demonstrated the dielectric properties of the polymer would also be altered by the strain-induced rearrangement of the polymer chains on the surface, such as in-plane reorientation of the phenyl group of polystyrene. As a result, the surface heterogeneity will increase and significantly reduce the carrier mobility of the OFETs.[38] In the current amorphous BST thin film, as the capacitance per unit area remains almost constant at different bending radii, it is safe to neglect the dielectric effects on the mobility change under bending. The stable dielectric properties of the BST thin film under bending suggest that it can be used as the universal dielectric layer for flexible transistors without SAM. The observed mobility increase while the device is under mild concave bending is attributed to the reduction of the distance between the pentacene molecules which further enhances charge hopping. On the other hand, the mobility will drop if we further reduce the bending radius. This is believed to be related to the degradation of the interface between the top electrodes and the pentacene, which results in higher contact resistance.

Based on the performance of the OFETs on a BST gate dielectric, we take a step further to bring the current OFETs to the basic logic circuit application by demonstrating their

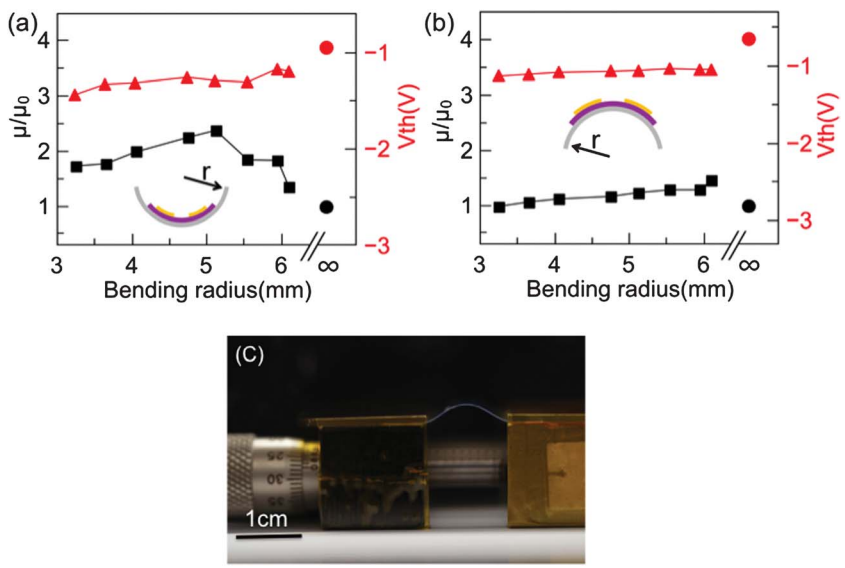


**Fig. 6** The change of mobility and threshold voltage of OFETs with (a) compressive and (b) tensile strain. The filled circles indicate the values without bending. (c) The picture of the bending test setup.

 

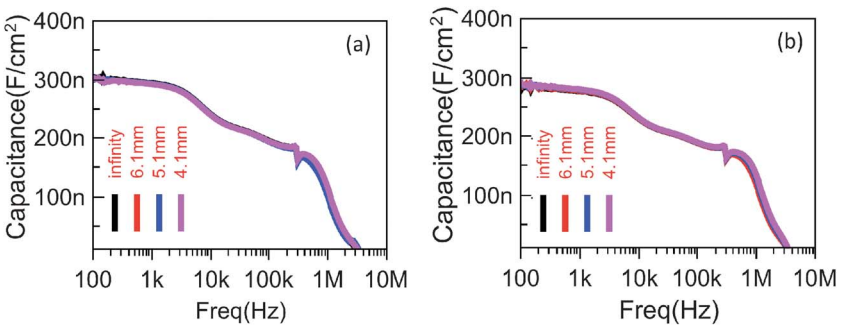


**Fig. 7** The capacitance–frequency measurements of the BST thin film under (a) compressive and (b) tensile strain in capacitor structure with different bending radii.

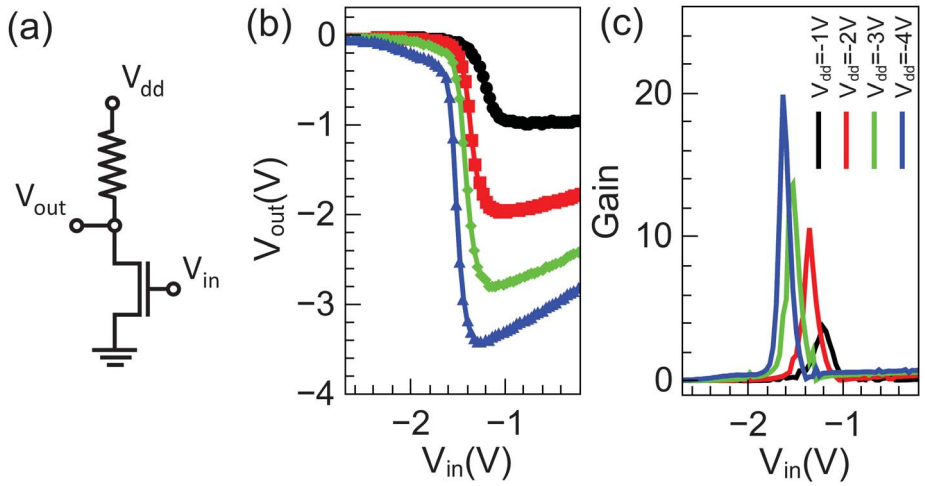


**Fig. 8** (a) The schematic circuit of the inverter device. (b) The $V_{out}$ and (c) gain of inverter devices as a function of $V_{in}$.

inverter applications as they are the basic components of almost all the integrated circuits. Different from the complementary inverter, we connected a 330 MΩ resistor to the transistor as shown in the schematic diagram in Fig. 8(a). Fig. 8(b) and (c) give the $V_{out}$ and the gain for each $V_{dd}$, ranging from −1 to −4 V, respectively. The inverters show good switching behavior, which can switch the high potential $V_{in}$ to the low voltage output and *vice versa*. The gain of the current inverters, defined as the maximum value of the slope of the $V_{in}$ *versus* $V_{out}$ curve, shows a maximum value around 20 and this is highly comparable with some of the depleted mode inverters[39] and complementary inverters.[30,40]

## Conclusions

In summary, we demonstrated the feasibility of a low temperature UV-ozone derived BST thin film as the high-*k* dielectric of the flexible OFET. The XPS results suggest that the chemical states of elements in the thin film are similar to the high temperature annealed thin film. The proposed layer-by-layer UV-ozone treatment is an effective way to solidify the thin film instead of high temperature annealing. The high resolution TEM image confirms the amorphous characteristic of BST with the total thickness of around 28 nm. On top of the BST thin film, the thermally evaporated pentacene layer shows island morphology in S–K growth mode. The current OFET with BST dielectric can be operated at a voltage smaller than 3 V with a mobility of 0.252 $cm^2 V^{-1} s^{-1}$ and the inverter gain of around 20 can be achieved. This SAM-free BST thin film can be derived under atmospheric air conditions and shows no capacitance variation under both concave and convex bending; these findings demonstrate the great application potential in large area fabrication of organic transistor and sensor devices.

## Acknowledgements

This work is supported by the HKU funding under 201109159013 and PolyU funding under Code: A-PL51/A-PM21. The authors thank the help of Electron Microscope Unit (EMU) of The University of Hong Kong.

## Notes and references

1 S. M. Wang, C. W. Leung and P. K. L. Chan, *Org. Electron.*, 2010, **11**, 990.
2 T. Sekitani, T. Yokota, U. Zschieschang, H. Klauk, S. Bauer, K. Takeuchi, M. Takamiya, T. Sakurai and T. Someya, *Science*, 2009, **326**, 1516.

3 H. Klauk, U. Zschieschang, J. Pflaum and M. Halik, *Nature*, 2007, **45**, 745.
4 M. Novak, A. Ebel, T. Meyer-Friedrichsen, A. Jedaa, B. F. Vieweg, G. Yang, K. Voitchovsky, F. Stellacci, E. Spiecker, A. Hirsch and M. Halik, *Nano Lett.*, 2011, **11**, 156–159.
5 Y. Zhao, C. Di, X. Gao, Y. Hu, Y. Guo, L. Zhang, Y. Liu, J. Wang, W. Hu and D. Zhu, *Adv. Mater.*, 2011, **23**, 2448.
6 O. Acton, G. Ting, H. Ma, J. W. Ka, H. L. Yip, N. M. Tucker and A. K. Y. Jen, *Adv. Mater.*, 2008, **20**, 3697.
7 P. H. Wobkenberg, J. Ball, F. B. Kooistra, J. C. Hummelen, D. M. De Leeuw, D. D. C. Bradley and T. D. Anthopoulos, *Appl. Phys. Lett.*, 2008, **93**, 013303.
8 K. Kuribara, H. Wang, N. Uchiyama, K. Fukuda, T. Yokota, U. Zschieschang, C. Jaye, D. Fischer, H. Klauk, T. Yamamoto, K. Takimiya, M. Ikeda, H. Kuwabara, T. Sekitani, Y. L. Loo and T. Someya, *Nat. Commun.*, 2012, **3**, 723.
9 E. P. Plueddemann, *Silane Coupling Agents*, Plenum Press, New York, 2nd edn, 1991.
10 S. A. DiBenedetto, A. Facchetti, M. A. Ratner and T. J. Marks, *Adv. Mater.*, 2009, **21**, 1407.
11 Y. M. Park, J. Daniel, M. Heeney and A. Salleo, *Adv. Mater.*, 2011, **23**, 971.
12 X. H. Zhang, B. Domercq, X. Wang, S. Yoo, T. Kondo, Z. L. Wang and B. Kippelen, *Org. Electron.*, 2007, **8**, 718.
13 X. H. Zhang, S. P. Tiwari, S.-J. Kim and B. Kippelen, *Appl. Phys. Lett.*, 2009, **95**, 223302.
14 S. P. Tiwari, Z. Xiao-Hong, W. J. Potscavage and B. Kippelen, *Appl. Phys. Lett.*, 2009, **95**, 223303.
15 Z. R. Wang, J. Z. Xin, X. C. Ren, X. L. Wang, C. W. Leung, S. Q. Shi, A. Ruotolo and P. K. L. Chan, *Org. Electron.*, 2012, **13**, 1223.
16 C. D. Dimitrakopoulos, S. Purushothaman, J. Kymissis, A. Callegari and J. M. Shaw, *Science*, 1999, **283**, 822.
17 C. Y. Wei, S. H. Kuo, Y. M. Hung, W. C. Huang, F. Adriyanto and Y. H. Wang, *IEEE Electron Device Lett.*, 2011, **32**, 90.
18 C. D. Dimitrakopoulos, I. Kymissis, S. Purushothaman, D. A. Neumayer, P. R. Duncombe and R. B. Laibowitz, *Adv. Mater.*, 1999, **11**, 1372.
19 J. Li, D. Liu, Q. Miao and Y. Feng, *J. Mater. Chem.*, 2012, **22**, 15998.
20 K. H. Lee, K. Lee, M. S. Oh, J. M. Choi, S. Im, S. Jang and E. Kim, *Org. Electron.*, 2009, **10**, 194.
21 O. Acton, G. G. Ting II, H. Ma, D. Hutchins, Y. Wang, B. Purushothaman, J. E. Anthony and A. K. Y. Jen, *J. Mater. Chem.*, 2009, **19**, 7929.
22 G. D. Wilk and B. Brar, *IEEE Electron Device Lett.*, 1999, **20**, 132.
23 M. Hasan, J. Rho, S. Y. Kang and J.-H. Ahn, *Jpn. J. Appl. Phys.*, 2010, **49**, 05EA01.
24 M. E. Pilleux, C. R. Grahmann and V. M. Fuenzalida, *J. Am. Ceram. Soc.*, 1994, **77**, 1601.
25 S. M. Mukhopadhyay and T. C. S. Chen, *J. Mater. Res.*, 1995, **10**, 1502.
26 B. G. Frederick, G. Apai and T. N. Rhodin, *J. Am. Chem. Soc.*, 1987, **109**, 4797.
27 D. J. Jacob, *Introduction to Atmospheric Chemistry*, Princeton University Press, Princeton, NJ, 1999.
28 U. Haas, H. Gold, A. Haase, G. Jakopic and B. Stadlober, *Appl. Phys. Lett.*, 2007, **91**, 043511.
29 T. Sekitani, Y. Kato, S. Iba, H. Shinaoka, T. Someya, T. Sakurai and S. Takagi, *Appl. Phys. Lett.*, 2005, **86**, 073511.
30 S. P. Tiwari, V. R. Rao, T. Huei Shaun, E. B. Namdas and S. G. Mhaisalkar, presented at the 14th International Symposium on VLSI Technology, Systems, and Applications (2007 VLSI-TSA).
31 H. Klauk, M. Halik, U. Zschieschang, F. Eder, G. n. Schmid and C. Dehm, *Appl. Phys. Lett.*, 2003, **82**, 4175.
32 M. H. Yoon, H. Yan, A. Facchetti and T. J. Marks, *J. Am. Chem. Soc.*, 2005, **127**, 10388.
33 M. Mizukami, N. Hirohata, T. Iseki, K. Ohtawara, T. Tada, S. Yagyu, T. Abe, T. Suzuki, Y. Fujisaki and Y. Inoue, *IEEE Electron Device Lett.*, 2006, **27**, 249.
34 J. H. Na, M. Kitamura, D. Lee and Y. Arakawa, *Appl. Phys. Lett.*, 2007, **90**, 163514.
35 Y. W. Choi, I. D. Kim, H. L. Tuller and A. I. Akinwande, *IEEE Trans. Electron Devices*, 2005, **52**, 2819.
36 H. Sirringhaus, *Proc. IEEE*, 2009, **97**, 1570.
37 Y. Xu, M. Benwadih, R. Gwoziecki, R. Coppard, T. Minari, C. Liu, K. Tsukagoshi, J. Chroboczek, F. Balestra and G. Ghibaudo, *J. Appl. Phys.*, 2011, **110**, 104513.
38 A. N. Sokolov, Y. Cao, O. B. Johnson and Z. Bao, *Adv. Funct. Mater.*, 2011, **22**, 175.
39 Y. Zhou, S. T. Han, Z. X. Xu and V. A. L. Roy, *J. Mater. Chem.*, 2012, **22**, 4060.
40 J. W. Chang, C. G. Wang, C. Y. Huang, T. D. Tsai, T. F. Guo and T. C. Wen, *Adv. Mater.*, 2011, **23**, 4077.

 